Proceedings of the 3rd International Conference on Software Engineering and Machine Learning
DOI: 10.54254/2755-2721/150/2025.22694

"Forward or Backward?" - Effects of Center of Gravity Position on Gliding Distance of Unpowered Gliders

Yaning Zhang

International Department of Beijing No.35 High School, Beijing, China
yxthsier@126.com

Abstract: To investigate how to maximize the gliding distance of unpowered gliders through center of gravity adjustment, this study established a one-dimensional transient mathematical model describing the glider's pitch motion based on fundamental mechanical principles. The actual lift and drag coefficient curves were obtained through experimental testing. Using these empirical curves, the optimal center of gravity position was derived under fixed conditions of launch height, angle, and velocity. The effectiveness of this conclusion was qualitatively verified through final validation experiments.

Keywords: gliding, center of gravity position, dynamic analysis, numerical simulation, moment of inertia, lift coefficient

1. Introduction

A glider is a paper airplane, which is a light kind of a glider that is without a power unit. Basic mechanical analysis shows that three forces, such as lift, drag, and gravity, all act at the same time on it when it is in flight. Gliders do not have a continuous thrust like powered aircraft. Therefore, they must be able to sustain more upward lift to counteract the downward gravitational motion if longer distances are to be achieved in flight under identical mass and initial velocity conditions. Lift is mostly accompanied by drag; consequently, it is hard to raise lift without raising drag. The question now is, how can we maximize the flight distance of a glider? It was this simple question that aroused my curiosity to study gliding patterns. I suspected that under this common phenomenon lies much richer physical principle that needs to be looked into.

The survey on literature proved that most of the researchers or investigators have used toy gliders and paper airplanes as model aircraft. For example, they Wang Wei et al. [1] carried out an experiment on the impact of throwing angle and center of gravity position on the flight duration of Suzanne paper airplanes. After the center of mass had been determined by means of formulas and needle-point methods, mathematical models and state function equations for that property were established, solving the problem with MATLAB software. Paper airplane motion patterns were studied and trajectory equations were set up in the research by Gao Ji et al. [2]. Optimal launch angles were derived through coordinate systems and numerical solutions, developed throwing models, and obtained instantaneous velocities in glide by Newton's Second Law. The researchers obtained the result from the relationship between glide distance and lift coefficient aided by the transformation of potential and kinetic energies and energy conservation principle. Furthermore, the relationship between instant velocity, angle of attack, and lift coefficient was considered. Paper airplane flight principle and correlation between flight distance regarding various factors are what Shang Yuxiang

DOI: 10.54254/2755-2721/150/2025.22694

[3] discussed in theoretical mechanics, with the ultimate outcome being expressions for the distance of flight for a paper airplane. Dong Xiaohong et al. [4] study the principle of paper airplane flight on the basis of force analysis with Bernoulli's principle. AutoCAD software was used for the diagrams of force analysis, and mathematical models of optimal launch angles were established. A control experiment was performed, the flight data was marked with real-life MATLAB graphics, and the optimum launch strategy is developed. Natalia COOK [5] performed repeated experiments of paper airplane flight paths and design features related to predictive models of trajectory and stability mode (longitudinal, directional, and lateral) in which she recorded flight distances and time using 20 designs. Results revealed that there was a strong relationship with fuselage depth and performance in flight; the longitudinal and directional modes of stability seemed to depend on fuselage depth. This means that the contribution made toward the flight characteristics by the longitudinal mode is most significant. Simulations of flight for the best paper airplanes were done using equations of motion as developed by Stengel (2004).

In these studies, most researchers indicated that moving the glider's center of gravity forward to create "longitudinal static stability" effectively improves longitudinal attitude stability and flight distance. However, precise quantitative results determining optimal forward center of gravity displacement were generally lacking. Furthermore, most studies simplified their derivations by approximating transient conditions as steady-state and often arbitrarily selected parameters for their mathematical models, typically using fixed lift/drag coefficients without fully considering the effects of attitude changes on relevant parameters during flight.

Accordingly, this paper attempts to establish a one-dimensional non-steady-state glider model that accounts for time-varying factors to accurately predict relationships between flight trajectories and initial conditions. Simple, accessible experimental equipment was used to conduct zero-dimensional and one-dimensional experiments to verify the accuracy of the physical model and provide precision corrections. Finally, under conditions of unchanged lift structure, launch height/angle, and initial velocity, an optimal center of gravity position was determined.

This research follows the technical approach of "theoretical analysis → preliminary experiments to reproduce key phenomena → theoretical model modification based on phenomena → numerical solution of theoretical mathematical models → analysis of main parameters' effects on phenomena → optimization of main parameters → further experimental verification." Starting from basic mechanical analysis, the study attempts to establish theoretical models describing the phenomena, using simple experiments to verify the models' rationality and improve their accuracy. The theoretical models are then numerically solved and optimized to determine the optimal center of gravity position, followed by verification experiments, forming two closed iteration loops between theory and experiment.

2. Basic theoretical model

2.1. Zero-dimensional projectile model

Consider a point mass sphere and first investigate its trajectory under the conditions of air resistance. When the sphere is thrown into the air with initial velocity v_0, an initial angle θ, and height h_0, it will be subject to the combined effects of gravity and air resistance. The force of gravity always acts straight down in the vertical direction, while the force of air resistance opposes the direction of motion and can be broken down into components in the X and Y directions, as illustrated in Figure 1.

DOI: 10.54254/2755-2721/150/2025.22694

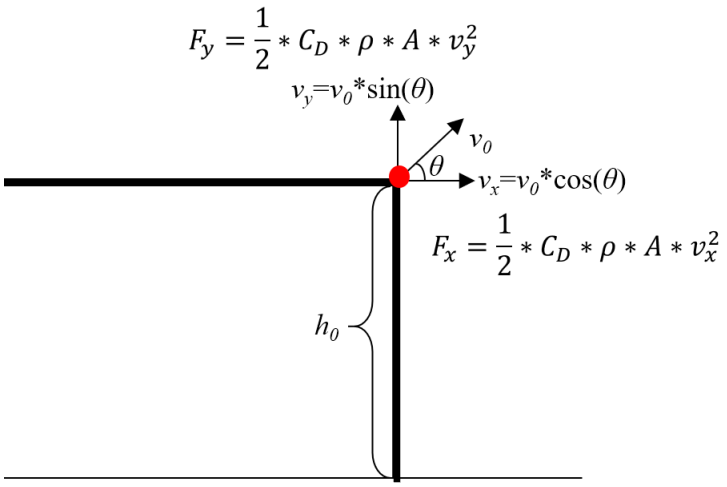

Figure 1: Schematic diagram of the air resistance on a 0-dimensional ball

The air resistance is calculated using formula (1):

$$F = \frac{1}{2} * Cd * v^2 * \rho * A \tag{1}$$

where Cd is the air resistance coefficient for a sphere, which can be taken as 0.47 [6]. This force can be decomposed into two perpendicular to forward components, along X and Y axes in a Cartesian coordinate frame, with the direction of motion considered positive in the X direction and upward motion taken as the positive Y direction.

According to Newton's Second Law, the acceleration along X and Y axes equal the force divided by the mass of the sphere. Equations (2-5) show how explicit time-stepping discretization calculates the acceleration components and their corresponding velocity components and new coordinate positions at each moment.

$$a_x = -\frac{F_x}{m} \tag{2}$$

$$a_y = -\frac{F_y}{m} - g \tag{3}$$

$$v_{t+1} = v_t + a * \Delta t \tag{4}$$

$$S_{t+1} = S_t + (v_t + \frac{1}{2} * a_t * \Delta t) * \Delta t \tag{5}$$

By continuously updating the components of the velocity vector, v_x and v_y, through time step Δt, and subsequently updating X and Y coordinates using these velocity components, the complete flight trajectory can be obtained. The Python code implementing trajectory calculation is as shown below (see Appendix 1) and results obtained will be presented together with experimental data in Chapter II.

2.2. One-dimensional glider launch model

We next try to stretch the zero-dimensional idea to one-dimensional situations. Not like the zero-dimensional circle, a glider makes lift besides having drag while flying, leading to more complicated force dealings. For now leaving out roll and yaw, and looking at just pitch, the glider is made simpler to nearly a one-dimensional model along its length direction, as seen in Figure 2.

DOI: 10.54254/2755-2721/150/2025.22694

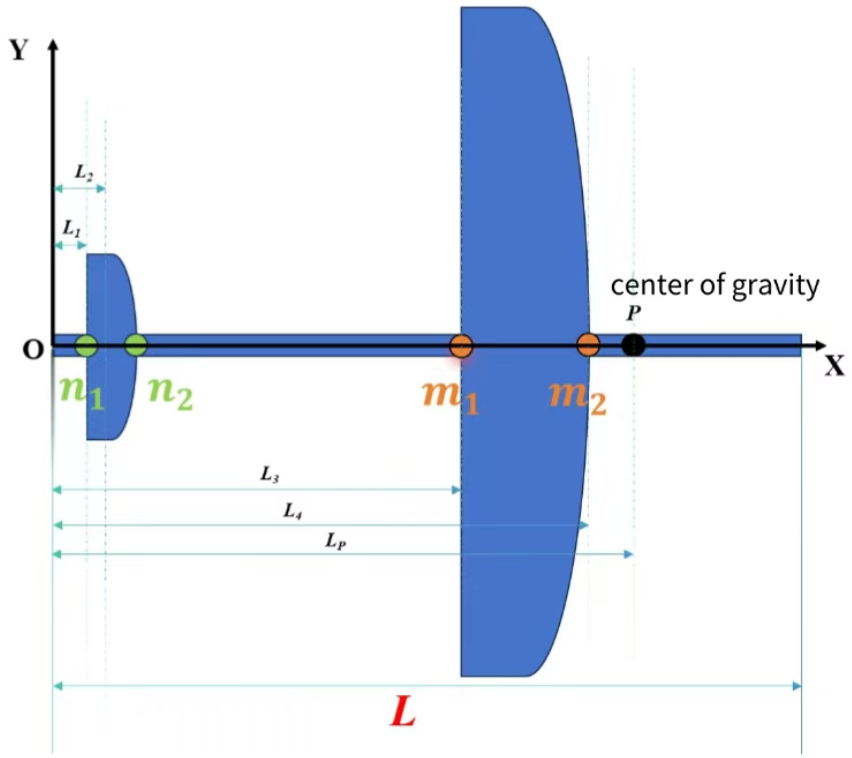

Figure 2: Simplified one-dimensional model of a glider

The main wing and tail wing are the elements primarily instrumental in lift and drag, center of gravity of the glider being at point P as shown in Figure 2. As the glider is in the process of gliding, lift and drag produced will mainly depend upon velocity and angle of attack α. This one is the difference between the attitude angle θ (angle between the body of the aircraft and the ground) and the angle made by the velocity at present, which is φ as shown in Figure 3.

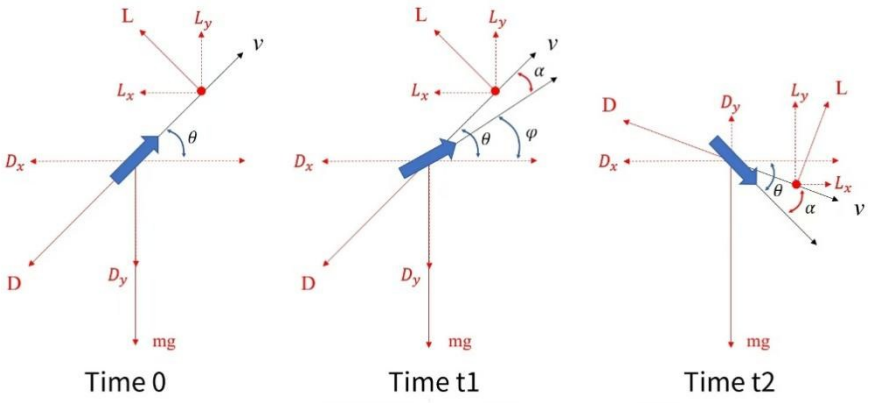

Figure 3: Schematic diagram of the angle of attack of a 1D glider model during flight

There are two main differences from the sphere flight model. First, during glider flight, when the total lift point produced by the main wing and tail wing does not coincide with the center of gravity P, an angular acceleration around the center of gravity will necessarily occur, meaning the glider's attitude angle changes during flight. Second, during flight, as the angle of attack and velocity continuously change, lift/drag coefficients cannot be treated as constants as in the sphere model. For the first issue, angular acceleration and angular displacement can be calculated numerically by

DOI: 10.54254/2755-2721/150/2025.22694

computing the lift magnitude to determine the rotational moment. However, lift calculation still depends on accurate determination of lift coefficients, leading to the core question: how to accurately obtain the glider's lift/drag coefficients under different angles of attack?

According to lift coefficient curves recorded in relevant literature [7], within the 0°-16° range, conventional wing lift and drag coefficients generally increase with increasing angle of attack, with optimal lift-to-drag ratio achieved at a 12° angle of attack, as shown in Figure 4.

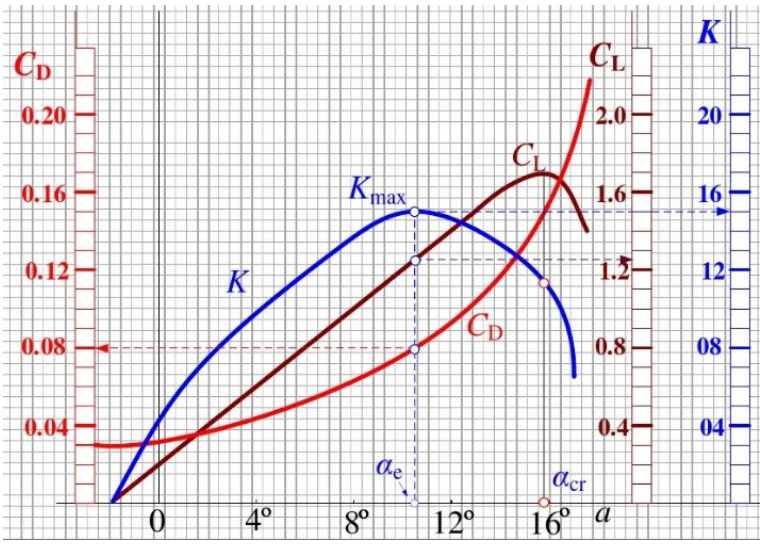

Figure 4: Variation of lift/drag coefficient of conventional wing with angle of attack

But these numbers may not be the same as the glider we used in our tests. So, I first thought of lift and drag amounts as fixed values while looking at the inertia of the glider, finding the total inertia by adding up the separate parts from the main wing, tail wing, and body then using this to calculate how much it turns, as seen in equations (6) and (7). Exact details and the Python code used can be found in Appendix 2 with the path of the glider calculated roughly like in Figure 5.

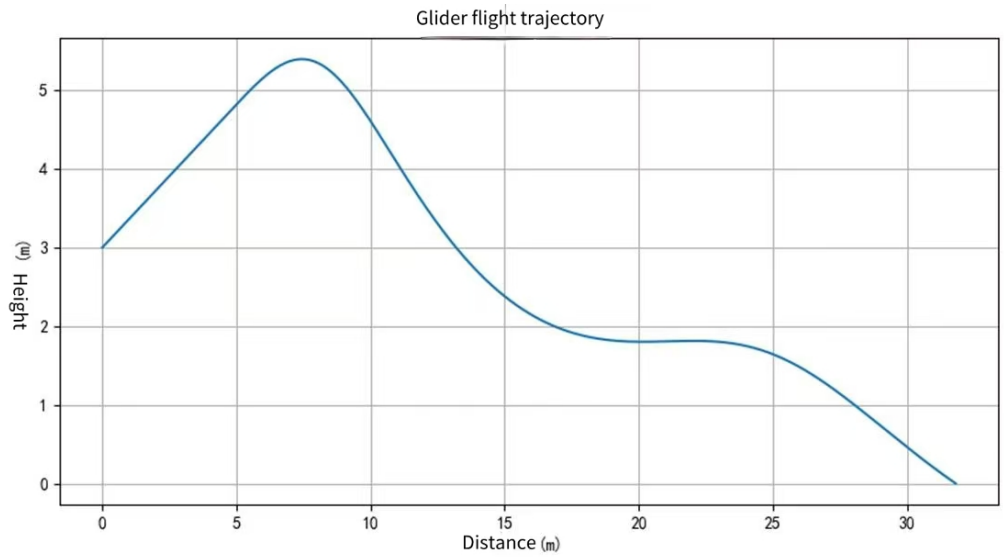

Figure 5: Glider flight trajectory under constant lift/drag coefficient conditions

One-dimensional moment of inertia calculation formula under constant density:

DOI: 10.54254/2755-2721/150/2025.22694

$$I = \rho \int_a^b r^2 dr \tag{6}$$

where r represents the distance from the mass point to the rotation axis, ρ is the one-dimensional linear density (constant), and a and b are the integration start and end points respectively.

Angular acceleration equals total torque divided by total moment of inertia:

$$a_\theta = \frac{F \cdot r}{I} \tag{7}$$

Here, $F \cdot r$ represents torque, which for the glider primarily consists of lift forces perpendicular to the attitude direction generated by the main wing and tail wing. I represents the total moment of inertia, obtained by summing the contributions from main wing, tail wing, and fuselage.

Since the angle of attack does not affect lift and drag coefficients in this case, the pitching motion caused by angular velocity is completely independent of the flight trajectory, making it impossible to investigate the impact of center of gravity position on flight performance. To study the effects of center of gravity position on flight performance and establish a mathematical model capable of predicting these effects, subsequent experimental data must be used to modify the lift/drag coefficients.

3. Preliminary experiments and results analysis

3.1. Zero-dimensional experiments

In theoretical analysis in Chapter I, zero-dimensional and one-dimensional projectile flight models were both proposed. The zero-dimensional model is relatively simple and has fewer external factors of influence; the parameters can be obtained relatively easily. Therefore, we designed and carried out first zero-dimensional experiments to check the dependability of the experimental apparatus. Different materials spheres were employed as zero-dimensional flying objects, launched by some projectile device.

3.1.1. Experimental setup

Two broad parts of the experimental set-up are the launch device and the measurement devices. The former gives the flying object (ball/glider) some initial velocity and mainly uses some elastic mechanism for power storage. In order to maintain consistency in the initial velocity of each launch, the launcher was marked with scales. Cameras were placed at the exit of the launcher so that the velocity of launch could be calculated by the displacement during the video frames. The angle of the launcher and the height from the ground, both are adjustable and it is shown in Fig. 6.

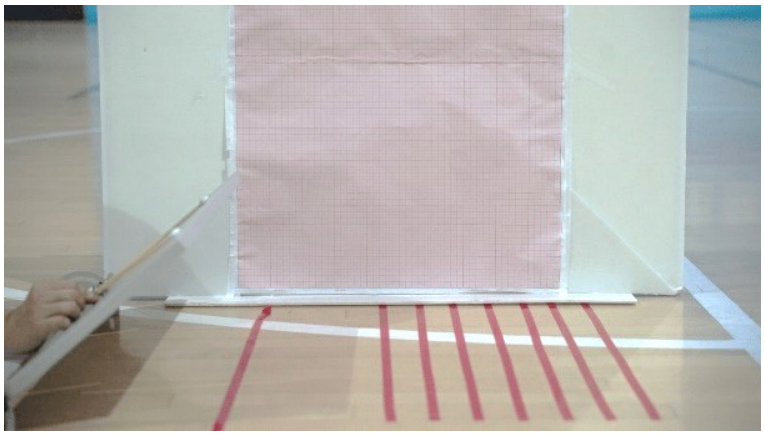

Figure 6: Catapult structure diagram

DOI: 10.54254/2755-2721/150/2025.22694

The devices used take the following key experimental data; distance, initial velocity, mass, and force measurements. The instruments used are in the categories of force gauges, vernier calipers, electronic balances, and measuring tapes as shown in Figure 7.

Figure 7: Various measuring devices (from left to right, dynamometer, vernier caliper, electronic balance, tape measure)

The measurement range and precision of various instruments are shown in Table 1.

Table 1: Measurement range and precision of various instruments

Instrument	Measurement Range	Precision	Physical Quantities Measured
Vernier Caliper	0-20 cm	0.1 mm	Ball diameter/Aircraft length/Spring extension length, etc.
Measuring Tape	0-20 m	1 mm	Flight distance/Launch height, etc.
Grid Paper	0-20 cm	0.5 cm	Initial launch velocity
Video	0-3600 s	1/30 s	Time
Electronic Balance	0-5 kg	0.01 g	Ball/Aircraft mass
Spring Force Gauge	0-50 N	0.1 N	Launch force
Protractor	0-180°	0.5°	Launch angle

Initial velocity is controlled by the spring's extension length, assuming that when the projectile mass remains constant and spring extension is identical, equal initial velocities can be provided. Initial velocity is measured using camera footage (30 FPS) set near the launcher, calculating displacement between adjacent video frames (1/30 s) using background grid paper, as shown in Figure 8.

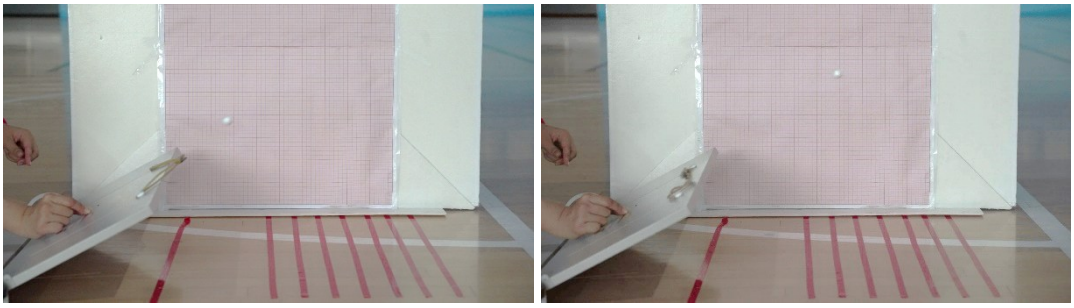

Figure 8: Schematic diagram of the method for measuring the initial velocity of a ball launch

Complete flight trajectories and distances are determined using measuring tape and wide-angle lenses set at a distance, as shown in Figure 9.

DOI: 10.54254/2755-2721/150/2025.22694

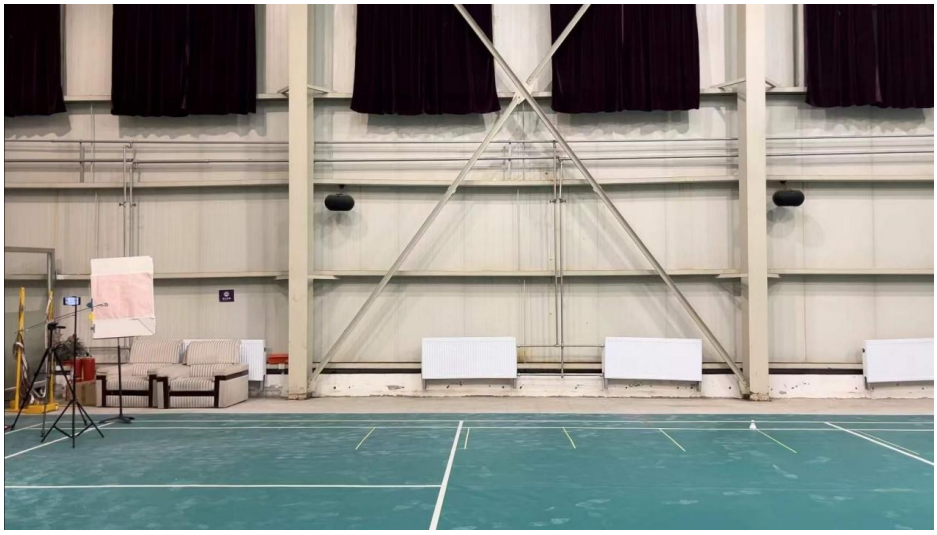

Figure 9: Distance measuring device and flight trajectory measuring device

3.1.2. Experimental Conditions

Experiments were conducted in an indoor gymnasium without wind. All balls used had a diameter of 2 cm (some foam balls were 1.9 cm due to manufacturing tolerance), with different materials as shown in Figure 10.

Figure 10: Three types of balls used in the 0-dimensional ball experiment (beech wood/stainless steel/polyethylene foam)

The main variables for zero-dimensional ball experiments are shown in Table 2.

Table 2: Variables in ball launch experiments

Variable Name			
Ball Material/Density	Stainless Steel (7980 kg/m³)	Beech Wood (620 kg/m³)	Polyethylene Foam (75 kg/m³)
Launch Angle (°)	10	20	30
Launch Force (N)	4	6	8

In order not to make too many experimental trials, a baseline condition was chosen: beech wood, 20°, 6N. When analyzing different variable effects, only one variable was changed while keeping others as baseline conditions. So, 3+3+3=9 groups of experiments were completed. Each group was tested ten times and the average taken as the final result.

DOI: 10.54254/2755-2721/150/2025.22694

3.1.3. Experimental Results

Nine groups of experiments were completed according to the above conditions. The experimental conditions and corresponding average results are shown in Table 3. The height in Table 3 is related to the launch angle and is not an independent variable.

Table 3: Statistical results of ball launch experiments

No.	Material	Angle (°)	Force (N)	Height (cm)	Average Initial Velocity (m/s)	Average Flight Distance (m)
1	Beech Wood	10	6	6	8.927986	2.1104
2	Beech Wood	30	6	15.6	7.931116	4.044
3	Beech Wood	40	6	18.4	7.866564	4.854
4	Beech Wood	20	6	10.7	8.331906	3.32
5	Foam	20	6	10.7	12.47468	1.656
6	Stainless Steel	20	6	10.7	3.209926	0.63
7	Beech Wood	20	4	10.7	7.010374	2.084
8	Beech Wood	20	8	10.7	11.57556	5.77
9	Beech Wood	20	10	10.7	12.50726	7.126

The Relative Standard Deviation (RSD) of the 10 groups of experimental results is shown in Figure 11. Most experimental results show standard deviations below 10%, indicating good overall repeatability. Experimental condition 5 shows larger flight distance standard deviation, likely because the lightweight foam ball's flight attitude may be affected by more complex air vortices, which cannot be simply described by the mechanical formulas derived in this paper.

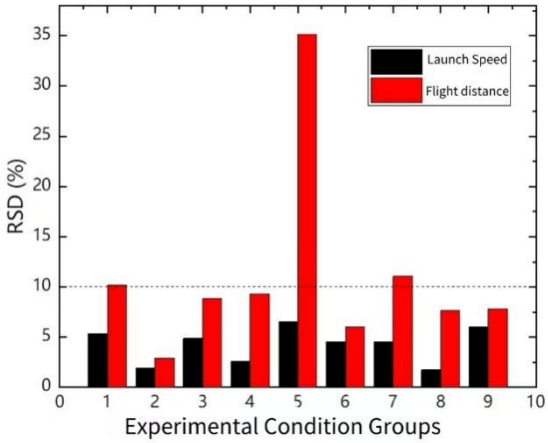

Figure 11: Standard deviation analysis of ball ejection test results

3.1.4. Results analysis and comparison

First, the transient calculations from the zero-dimensional theoretical model were implemented using Python software. The comparison between calculated flight distances and actual measured distances is shown in Figure 12.

DOI: 10.54254/2755-2721/150/2025.22694

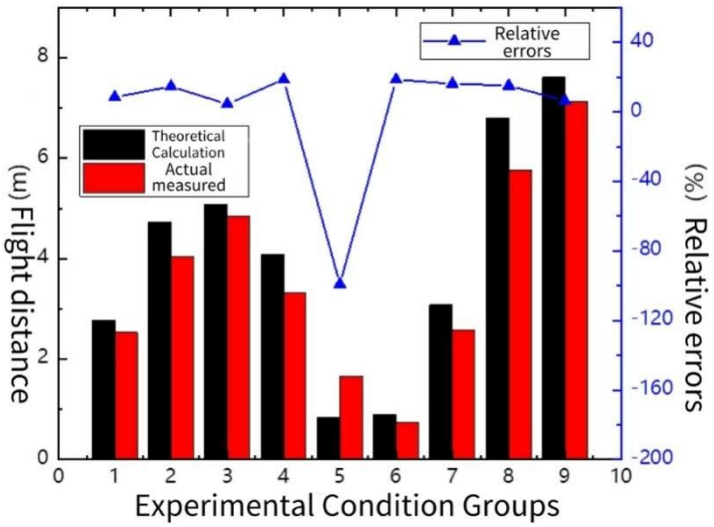

Figure 12: Comparison of theoretical calculation value and actual measurement value

Most theoretical values show good agreement with actual measurements, with relative errors generally not exceeding 20% (based on theoretical values), indicating high accuracy of this theoretical model in describing low-speed motion and good precision of the entire measurement system.

Yet, some states show bigger mistakes, like state 5, where the error gets to -95%. First look shows this is because the polyethylene foam ball is very light which makes it have too much speed at the start, possibly causing more complicated aerodynamic things like swirls, turbulence, and vortex streets during flight, which can't be shown by the easy theory.

3.2. One-dimensional experiments

3.2.1. Experimental setup

Compared to the ball projectile experiments, the one-dimensional glider experiments are essentially the same, with the primary experimental object changed to a laterally symmetrical wooden glider, as shown in Figure 13(a). A method of suspension wire was added to measure the center of gravity position, as shown in Figure 13(b); small rubidium magnets were used to be put into effect as well for adjusting the center of gravity position of the aircraft, as shown in Figure 13(c).

(a)

DOI: 10.54254/2755-2721/150/2025.22694

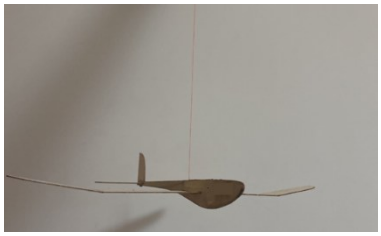

(b)

(c)

Figure 13: One-dimensional experimental object. (a) Wooden glider; (b) Suspension wire method for measuring the center of gravity; (c) Neodymium magnet for adjusting the center of gravity

3.2.2. Inverse problem theoretical model

The glider flight videos were processed frame by frame using Tracker software to obtain approximate center of mass positions and attitude vectors in each frame, as shown in Figure 14(a). Mathematical models were then established by analyzing three consecutive frames from the flight trajectory, as shown in Figure 14(b).

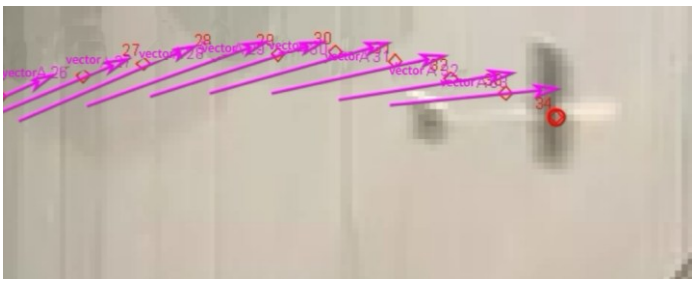

(a)

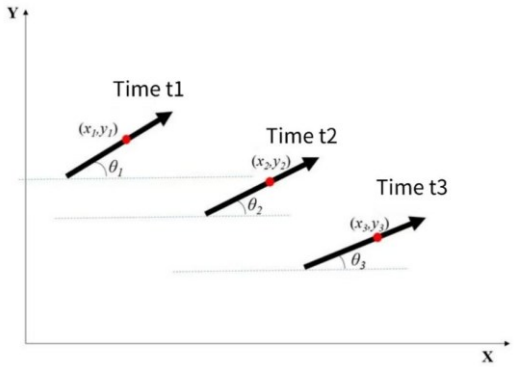

(b)

Figure 14: Data processing method for inverting lift and drag coefficients from experimental data. (a) Center of mass position and attitude vector extracted from Tracker; (b) Schematic diagram of attitude changes in 3 consecutive frames

DOI: 10.54254/2755-2721/150/2025.22694

Analysis of three consecutive images provides approximate glider center of mass coordinates and angle with the ground (attitude angle), as shown in Figure 14(b). Difference formulas were then used to express velocity and acceleration at time t_2, as shown in equations (8)-(13).

$$v_{x2} = \frac{1}{2}\left(\frac{x_3 - x_2}{\tau} + \frac{x_2 - x_1}{\tau}\right) \tag{8}$$

$$v_{y2} = \frac{1}{2}\left(\frac{y_3 - y_2}{\tau} + \frac{y_2 - y_1}{\tau}\right) \tag{9}$$

$$v_{\theta 2} = \frac{1}{2}\left(\frac{\theta_3 - \theta_2}{\tau} + \frac{\theta_2 - \theta_1}{\tau}\right) \tag{10}$$

$$a_{x2} = \frac{\frac{x_3 - x_2}{\tau} - \frac{x_2 - x_1}{\tau}}{\tau} \tag{11}$$

$$a_{y2} = \frac{\frac{y_3 - y_2}{\tau} - \frac{y_2 - y_1}{\tau}}{\tau} \tag{12}$$

$$a_{\theta 2} = \frac{\frac{\theta_3 - \theta_2}{\tau} - \frac{\theta_2 - \theta_1}{\tau}}{\tau} \tag{13}$$

In the above equations, τ represents the frame interval time (1/30 s). Then, following equations (2-3, 6), forces F_{x2} and F_{y2} in X and Y directions and corresponding rotational moment M_2 can be easily calculated using acceleration, glider mass, and total moment of inertia. Since lift and drag generally refer to forces along the velocity direction, another trigonometric transformation along the velocity angle is required.

The velocity angle is also given in difference form:

$$\varphi_2 = 1/2(\arctan\left(\frac{y_3 - y_2}{x_3 - x_2}\right) + \arctan\left(\frac{y_2 - y_1}{x_2 - x_1}\right)) \tag{14}$$

This allows calculation of lift and drag at time t_2 as shown in equations (15, 16).

$$F_{L2} = F_{y2} \times \cos\left(\varphi_2\right) - F_{x2} \times \sin\left(\varphi_2\right) \tag{15}$$

$$F_{D2} = -F_{x2} \times \cos\left(\varphi_2\right) - F_{y2} \times \sin\left(\varphi_2\right) \tag{16}$$

Having obtained the values for lift and drag, these are the values that are substituted into equation (1) to determine the coefficients of lift and drag at that instant. It should be noted that in calculating the coefficients of lift and drag, it is the component of the input force in those directions that gravitational effects contribute to and, therefore, must be subtracted from F_{L2} and F_{D2} as represented in Equations (17, 18).

$$F = \frac{1}{2} * Cd(or\ Cl) * v^2 * \rho * A \tag{1}$$

$$F_{L2}^{'} = F_{L2} + mg * \cos\left(\varphi_2\right) \tag{17}$$

$$F_{D2}^{'} = F_{D2} - mg * \sin\left(\varphi_2\right) \tag{18}$$

Here, area A is taken as the addition of main wing and tail wing areas, and velocity v is taken as the addition of v_{x2} and v_{y2} vectors.

In addition, the exact lift point position can be calculated backwards from the rotational moment that is obtained by image processing, as shown in equation (19).

DOI: 10.54254/2755-2721/150/2025.22694

$$r = \frac{M_2}{F_{x2} \times \sin(\theta_2) + F_{y2} \times \cos(\theta_2)} \tag{19}$$

Complete code is shown in Appendix 3.

3.2.3. Experimental results

Initially, two small rubidium magnets were placed at the glider's original center of gravity position, without adjusting the center of gravity position. Subsequently, 10 groups of launch experiments were conducted with different initial conditions by varying launch angles and forces. Each group was repeated several times. During launches, lateral deviation sometimes occurred due to insufficient balance adjustment of the glider. As such flight processes violated this paper's one-dimensional assumption, only experimental results with minimal lateral flight trajectory deviation were selected for data processing from each round of experiments. Videos showing significant deviation were not used. Finally, 15 videos were selected for point tracking and data processing.

Taking the processed results from one experiment as an example, Figure 15(a) shows the changes in angle of attack α, attitude angle θ, and velocity angle φ with flight time (horizontal axis shows frame numbers), while Figure 15(b) shows X and Y direction velocity changes over time.

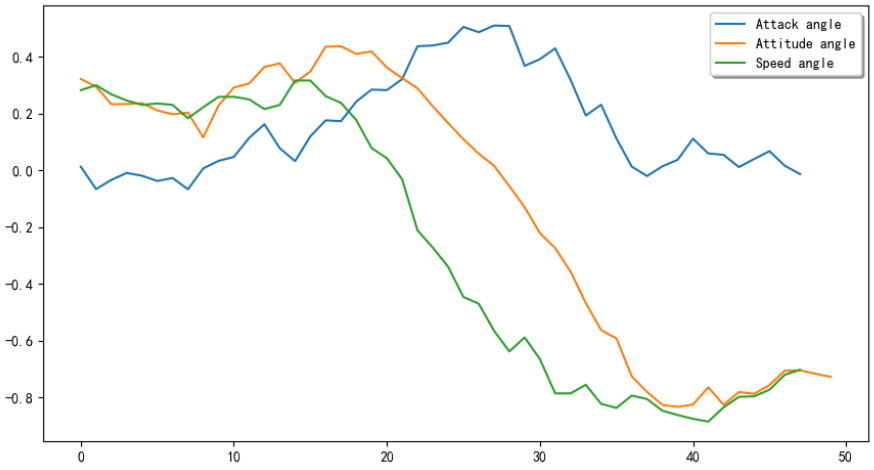

(a)

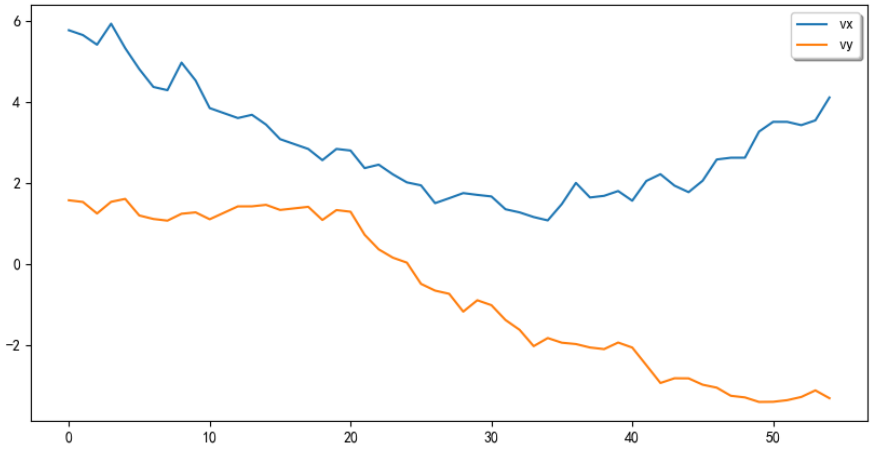

(b)

Figure 15: Flight parameters change over time. (a) Attitude angle, velocity angle, and angle of attack change over flight time; (b) X-direction velocity and y-direction velocity change over flight time

DOI: 10.54254/2755-2721/150/2025.22694

In Figure 15, it can be seen that for the first 20 frames, both the attitude angle and the velocity angle are positive. These results can be attributed to the fact that the glider is steadily flying forward and the angle of attack is fluctuating around 0°. Such characteristics are related to "static stability", whereby the glider self-adjusts to maintain its attitude. However, beyond 20 frames, when the velocities in both x and y directions decay to some particular level, lift generated is not sufficient anymore, then velocity angle falls rapidly, followed by the fall of the attitude angle, and at the same time, the angle of attack rises promptly to indicate entry into the region of the stall. When the glider is in the stall region, it is not capable of maintaining the height, and it starts descending very steeply. Yet when the glider's descent hits a point, as downward velocity starts to pick up speed, potential energy changes to motion energy, which creates more lift and force on the wings, this can lead the glider to speed up in the forward direction, creating opposite force to level its angle, while also lowering angle of attack. You can see this in Figure 15 by higher forward velocity and lower angle of attack as well as angle after frame 35.

Due to low launch height, only one round of this "dive and pull-up" curve could appear in experiments before landing. However, it can be predicted that with sufficient launch height, this periodic variation of level flight → descent → level gliding → descent might repeatedly occur during the glider's flight.

3.2.4. Actual lift/drag curves

The 15 selected videos gave lift/drag coefficients which were integrated using interpolation and averaging methods as illustrated in Figure 16 to give these two curves, which are actually the aerodynamic performance of the experimental glider under low-speed conditions.

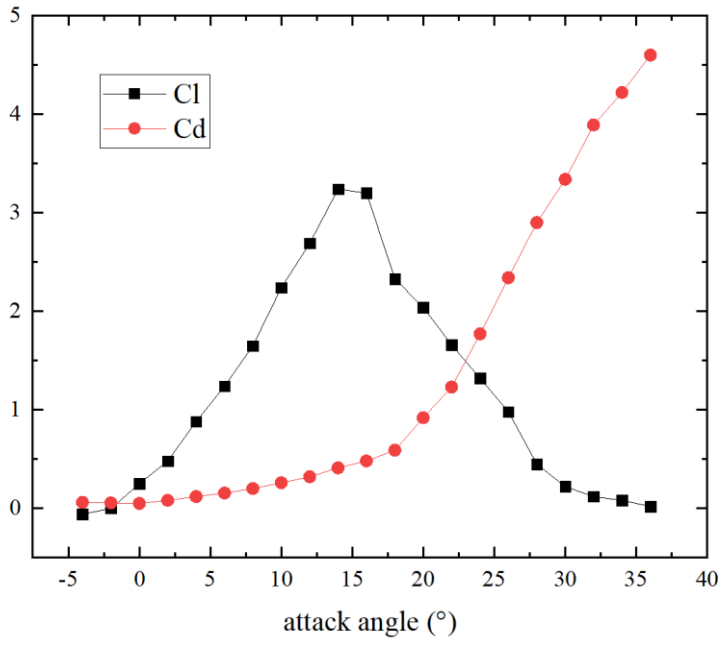

Figure 16: Variation of the experimentally measured average lift/drag coefficient with angle of attack

At larger angles of attack, the lift coefficient would show typical characteristics of initial increase followed by a fall. It achieved a maximum at about 14°. The drag coefficient would increase almost linearly within the first 18°, then almost exponential growth beyond 18°.

DOI: 10.54254/2755-2721/150/2025.22694

4. Optimization process and results analysis

Using the actual lift/drag coefficients obtained through experiments, we optimized the center of gravity position and launch angle. With fixed launch height of 1.5 m, launch angle of 30°, and launch velocity of 10m/s, the center of gravity position was adjusted within the range [0.16:0.19:0.001]m, varying from L_p = 0.16 m to L_p = 0.19 m as shown in Figure 2, with intervals of 0.001m. The calculated flight distances are shown in Figure 17.

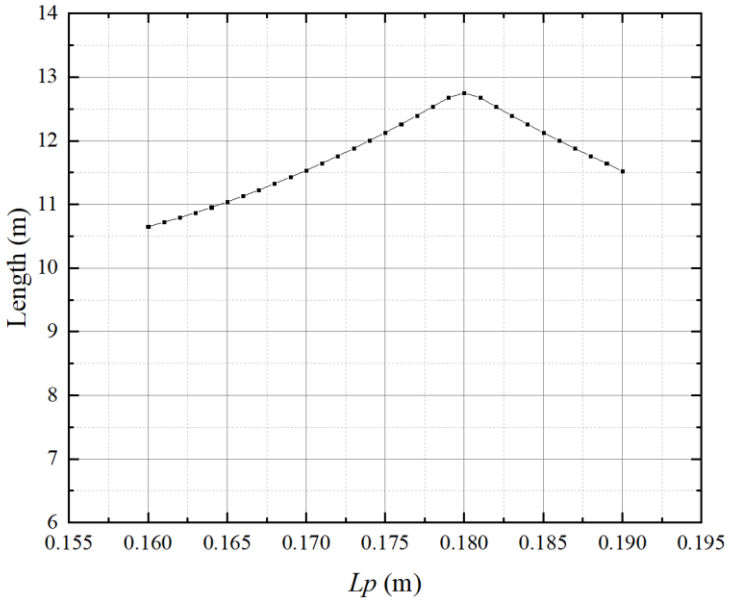

Figure 17: Flight distance changes with center of gravity position

The optimal center of gravity position is shown by Figure 17, which is 0.18m, or slightly posterior to the original 0.185m. The predicted flight trajectory for this optimal position is shown in Figure 18.

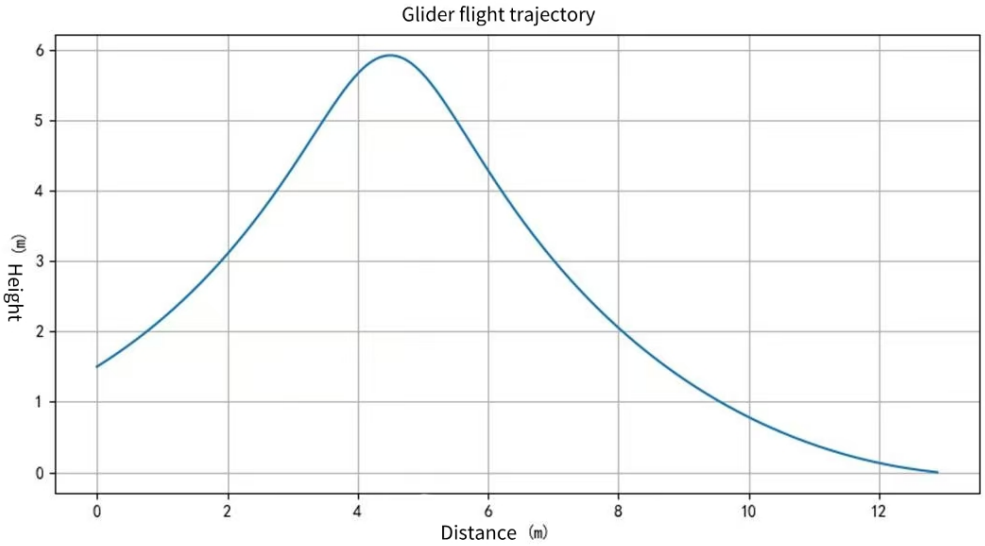

Figure 18: Flight curve of the best center of gravity position

Having obtained the theoretical results, the position of the center of gravity of the glider was readjusted, and a fresh set of tests was carried out. But, launches with optimized center of gravity

DOI: 10.54254/2755-2721/150/2025.22694

position did not yield statistically significant advantages in distance of flight. This was because the posterior shift in center of gravity made the glider considerably more unstable and difficult to maintain motion in a vertical plane; which easily led to lateral deviation. The errors essentially overtook the benefits that would accrue in flight distance by way of the adjustment in center of gravity. In the end, the rationality of this modification could not be verified successfully.

However, during this round of experiments, we discovered that forward center of gravity position could effectively extend the initial stable flight phase and improve flight stability with less lateral oscillation. However, gliders with forward center of gravity positions rarely exhibited "dive and pull-up" secondary gliding curves, usually resulting in direct descent. This might also relate to insufficient launch height of the current experimental apparatus, unable to provide adequate diving speed.

Gliders with slightly posterior center of gravity showed notably reduced controllability and stability, easily experiencing lateral oscillation. However, this configuration more readily produced secondary gliding curves. Combined with theoretical calculations, this can be attributed to shortened pitch rotation moment arm, requiring less force to level the glider's attitude. With good balance adjustment and absence of lateral deviation, this design might achieve longer flight distances.

However, limited by current experimental conditions' insufficient precision and poor reproducibility, accurate quantitative measurement results could not be provided.

5. Conclusions

Glider flight distance is simultaneously influenced by multiple factors including initial launch velocity, launch angle, center of gravity position, glider structure, and launch height. Through this research, we established a one-dimensional mathematical model capable of describing these influences, particularly determining the glider's actual lift/drag coefficients using simple experimental apparatus and incorporating the relationship between lift/drag coefficients and angle of attack, enabling quantitative study of center of gravity position's effect on flight trajectory. This model can ultimately find the optimal center of gravity position under fixed launch angle, velocity, and height conditions.

However, limited by current experimental equipment precision, while zero-dimensional sphere experiments showed good agreement with theoretical calculations, one-dimensional experiments encountered significant lateral deviation problems with posterior center of gravity movement, resulting in high variance in measured flight distances and preventing statistically significant experimental distinctions. Moreover, the glider may be affected by complex three-dimensional flow fields during flight, factors not fully describable by our one-dimensional model, warranting further quantitative analysis in future studies.

References

[1] *Wang Wei, Zhao Mingcheng. Analysis of Paper Airplane Air Time Based on Center of Gravity and Throwing Angle [J]. Journal of Heze University, 2022, 44(5):3.*

[2] *Gao Ji, Jia Wentai. Mathematical Model of Paper Airplane Throwing [J]. Technology Wind, 2019(25):1. DOI:CNKI:SUN:KJFT.0.2019-25-069.*

[3] *Shang Yuxiang. Research on Paper Airplane Flight Distance Using Theoretical Mechanics Knowledge [J]. Technology Wind, 2019(20):2. DOI:CNKI:SUN:KJFT.0.2019-20-193.*

[4] *Dong Xiaohong, Kang Ping. Mathematical Modeling of Optimal Angle and Center of Gravity Position for Paper Airplane Throwing [J]. Technology Wind, 2020(28):2. DOI:10.19392/j.cnki.1671-7341.202028091.*

[5] *Experimental Analysis of Paper Plane Flight Characteristics. Author: Natalia COOK, 43181737. THE UNIVERSITY OF QUEENSLAND ENGINEERING THESIS.*

[6] *John D. Anderson, Fundamentals of Aerodynamics [M], McGraw-Hill Science/Engineering/Math 2005.*

[7] *Aircraft Design Manual [M]. Aviation Industry Press, 2002.*